Comparative Study of Carbonaceous Materials as Catalyst Supports for the Enantioselective Hydrogenation of (E)-α-Phenylcinnamic Acid: Influence of the Support Acidity

Tran Si Bui Trung[*], Yeonwoo Kim[*], Sungho Kang[*], Hangil Lee[**], Sehun Kim[*]

[*]*Molecular-Level Interface Research Center, Department of Chemistry, KAIST, 305-701, Republic of Korea*

[**]*Department of Chemistry, Sookmyung Women's University, Seoul 140-742, Republic of Korea*

ABSTRACT: A systematic comparative study of carbonaceous materials as catalyst supports for the asymmetric heterogeneous hydrogenation of (E)-α-phenylcinnamic acid (PCA) was performed to investigate the influence of the supports on the reaction enantioselectivity. A series of Pd-based catalysts supported on activated carbon, graphene oxide (GO), or carbon nanotubes was prepared using deposition methods, and their physicochemical properties were characterized. The results demonstrated that the textural structure of the supports had a trivial effect on the enantiomeric excess (*ee*). The TGA, FT-IR, and TPD–NH_3 data revealed an abundance of acidic sites present on the Pd/GO catalyst, unlike the other catalysts, and these sites reduced the enantioselective hydrogenation of PCA. The effect of the support acidity on the enantioselectivity was ascribed to the preferential adsorption mode of cinchonidine (CD) on the GO surface *via* electrostatic interactions between the negatively charged oxygen functional groups present on the GO surface and the positively protonated amine groups present in the CD molecule.

1. INTRODUCTION

Heterogeneous catalyst systems have several advantages over homogeneous catalysts in that they are more easily recyclable and offer a higher yield. Heterogeneous systems could potentially provide green alternatives to stoichiometric processes and reduce the environmental impact of manufacturing. In a heterogeneous reaction, the catalyst support is critical to determine the catalytic performance [1–3]. Therefore, a thoroughly understanding the influence of the catalyst support in each application is essential for developing state-of-the-art catalysts with improved catalytic performances.

Activated carbon (AC) is one of the most extensively utilized supports for metal-based catalysts used in low-temperature reducing reactions, such as liquid phase heterogeneous hydrogenation reactions [4]. The recently discovered carbonaceous materials, including carbon nanotubes (CNTs) and graphene oxide (GO), show promise in a wide range of applications seeking to capitalize on their unique and fascinated properties [5,6]. CNTs and GO are broadly employed as heterogeneous catalyst supports because they possess a large surface area, provide good mechanical strength, and stable under harsh conditions [7,8]. Although AC, GO, and CNTs comprise layers of carbon atoms arranged in six-membered rings, their structures are distinct from one another. AC has an amorphous structure that consists of aromatic sheets and strips with slits of a variety of molecular dimensions that form porosity [9], whereas CNTs are composed of curved sp^2-hybridized carbon atoms arranged in an axial alignment of concentric cylindrical planes [10]. On the other hand, GO is a flat monolayer of carbon atoms tightly packed into a two-dimensional honeycomb lattice on which a variety of reactive oxygen functional groups are present [11]. The structural diversity of these carbonaceous supports results in different metallic active site structures and, consequently, induces distinctive catalytic behaviors.

The asymmetric heterogeneous hydrogenation of prochiral α,β-unsaturated carboxylic acids over cinchonidine (CD)–modified Pd-based catalysts has attracted enormous attention in recent decades due to the growing demand for enantiomerically pure compounds for use in various applications [12–14]. Among the most widely studied reactions is the enantioselective hydrogenation of (E)-α-phenylcinnamic acid (PCA), which has been intensively examined by Nitta and others [15–18]. Many factors that affect the enantioselectivity of the reaction, including the solvents [19], additives [20], or catalyst preparation conditions [21] have been investigated with the aim of enhancing the enantiomeric excess (*ee*) values. Activated carbon is a conventional catalyst support used in this type of reaction [22–25], and little effort has been applied toward the use of other carbonaceous materials, such as GO [26] or CNTs [27]. Moreover, no systematic studies have yet examined the effects of these carbonaceous supports on the enantioselectivity of the hydrogenation reaction of prochiral α,β-unsaturated carboxylic acids. Therefore, a comparison of these carbonaceous materials as catalyst supports for the hydrogenation of PCA could reveal the influence of the supports and clarify the mechanism underlying this reaction. These insights could assist the design of novel catalysts with enhanced enantioselectivity.

This work seeks fundamental insights into the role of the catalyst support in the enantioselectivity of the asymmetric

hydrogenation of PCA by systematically comparing the properties of carbonaceous material supports for Pd-based catalysts under similar catalyst preparation and hydrogenation reaction conditions. Pd-based catalysts supported on AC, GO, or CNTs were prepared using deposition methods and were characterized by a variety of approaches. The oxygen functional groups present on the supports were found to play a key role in determining the enantiodifferentiation properties.

2. EXPERIMENTAL SECTIONS

2.1. Pd catalyst preparation

Graphene oxide was synthesized using the modified Hummers method [28]. Supported palladium catalysts were prepared by the deposition–precipitation method using a $PdCl_2$ precursor. The $PdCl_2$ solution was prepared by ultrasonicating a mixture containing 25 mg $PdCl_2$ and 2 mL HCl (37%) in 10 mL H_2O for 20 minutes. In a typical preparation, 300 mg of the support (AC, GO, CNTs) were dissolved in 100 mL H_2O with ultrasonic treatment for 1 hour. The pH of the mixture was then adjusted to 10 by the addition of a 1 M Na_2CO_3 solution, followed by 30 minutes stirring. The $PdCl_2$ solution was then added to the suspension with stirring, and the pH of the mixture was adjusted to 10 again. After the pH adjustment, the mixture was stirred for 5 hours and then was heated at 80°C for 2 hours. The heat treatment magnified the acidity of the solution and promoted the hydrolysis process to form $Pd(OH)_2$, which anchored to the support surface [29,30]. The suspension was cooled to room temperature, and $NaBH_4$ dissolved in 20 mL H_2O was slowly dropped into it. The reaction was continued for 3 hours with stirring, and the black precipitate was filtered, washed 5 times with water (50 ml each time), dried overnight under ambient atmosphere in an oven (110°C), and stored for use.

2.2. Hydrogenation reaction

The solvent used in the hydrogenation reactions was wet 1,4-dioxane (containing 2.5% double-distilled water). Each reaction was repeated at least 3 times to obtain the average *ee* value. The hydrogenation reactions were carried out using procedures conducted with or without the pretreatment [31]. The pretreatment procedure involved heating 15 mg of the catalyst with 2 mL solvent in a 25 mL glass bottle with magnetic stirring (1000 rpm) at 80°C for 30 minutes under a H_2 atmosphere supplied by a balloon. After the pretreatment process, a solution of 0.01 mmol CD in 1 mL solvent was added at 23°C. The mixture was stirred for 30 minutes, and then a solution of 0.25 mmol PCA in 2 mL solvent was added, followed by the injection of 0.03 mL BA. The slurry was stirred with magnetic agitation at 1000 rpm at 23°C under the H_2 atmosphere. After the hydrogenation reaction had finished (8–12 hours). The product was esterified to produce the methyl ester, and the *ee* values were determined by HPLC using a chiral Chiralcel OD-H (Daicel) column.

3. RESULTS AND DISCUSSION

3.1. Characterization of the synthesized Pd-based carbonaceous supports

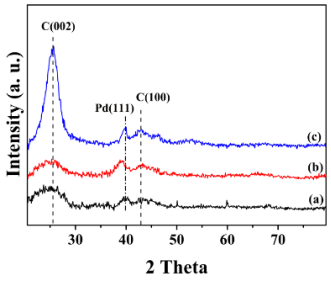

Figure 1. XRD patterns of the prepared catalysts (a) Pd/AC, (b) Pd/GO, and (c) Pd/CNTs.

The X-ray diffraction patterns of the Pd-based catalysts prepared with different carbonaceous supports were collected over the range 20°–80° to study the crystalline structures. As shown in Figure 1, diffraction peaks at 26° and 43° were observed in all catalysts and were assigned to the typical (002) and (100) planes of the hexagonal graphite structure, respectively. In the Pd/GO catalyst, these peaks indicated that GO was reduced partially to graphene sheets during the catalyst preparation steps, and the graphene sheets restacked to form an ordered crystalline structure [32]. The three synthesized catalysts exhibited characteristic diffraction peaks at 2θ=40°, which corresponded to the (111) crystalline plane of the *fcc* Pd nanoparticles (JCPDS #46-1043). It should be noted that this peak was broader in the Pd/AC and Pd/GO catalysts and sharper in the Pd/CNT catalyst, suggesting that the Pd nanoparticles present in the Pd/AC and Pd/GO catalysts were smaller than the Pd nanoparticles present in the Pd/CNT catalyst. In addition, this peak in the Pd/GO catalyst was shifted slightly toward lower diffraction angles due to the effects of the lattice strain, which increased the lattice parameter to a small degree [33].

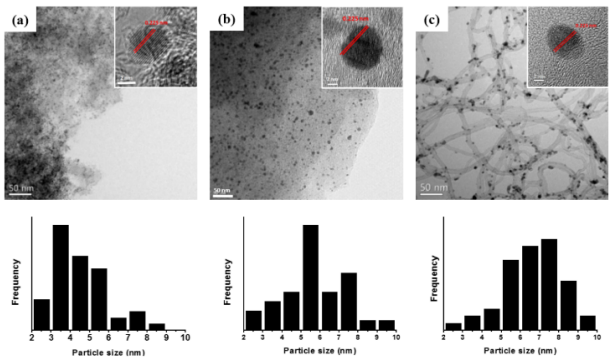

Figure 2. TEM images and (inset) HR-TEM images of the prepared Pd-based catalysts: (a) Pd/AC, (b) Pd/GO, or (c) Pd/CNTs, and their corresponding particle size distributions.

The morphologies and dispersions of the Pd nanoparticles in the prepared Pd-based catalysts were evaluated using bright-field TEM techniques. Representative

TEM images and the corresponding particle size distributions are shown in Figure 2. The insets show HR-TEM images of a randomly selected dark spot on the prepared Pd/AC, Pd/GO, or Pd/CNT catalysts, confirming that the particles were enclosed by facets with interplanar distances of 0.225nm, 0.228 nm, and 0.225 nm, respectively, based on the adjacent lattice fringes. These lattice parameters corresponded to the (111) plane of the *fcc* Pd crystal [34], in good agreement with the observations collected from the XRD data. The inset HR-TEM images also revealed that the Pd nanoparticles assumed sphere-like shapes in all of the catalysts. The Pd nanoparticles in the prepared catalysts were homogeneously decorated across the carbonaceous materials, and the particle size typically did not exceed 10 nm. The particle size distributions revealed that the Pd/AC catalysts included more numerous small (2–6 nm) Pd particles, whereas the Pd particles present on the Pd/CNTs catalysts were predominantly between 5 and 9 nm, in good agreement with the XRD data. The results obtained from the XRD and TEM analyses indicated that the Pd nanoparticles were successfully deposited onto the carbonaceous supports after the catalyst preparation process.

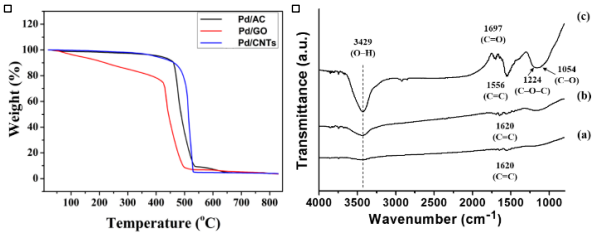

Figure 3. Left panel: TGA study of the prepared Pd-based catalysts: (black) Pd/AC, (red) Pd/GO, and (blue) Pd/CNTs. Right panel: FT-IR data of the prepared Pd-based catalysts: (a) Pd/CNTs, (b) Pd/AC, (c) and Pd/GO.

TGA studies were conducted over the temperature range between room temperature and 850°C to examine the thermal stability of the prepared Pd-based catalysts and to determine the practical Pd wt% loading. As shown in Figure 3 (left panel), the Pd/AC and Pd/CNT samples exhibited similar thermal behaviors. Initially, a small mass loss was observed as the temperature increased to 450°C; however, the TGA curves rapidly dropped to 5%wt within the temperature range 450–600°C, which was attributed to the weight loss due to the removal of the carbon component. By contrast, the Pd/GO catalysts displayed over 15% weight loss at 300°C as a result of the removal of oxygen-functional groups, such as C–O, C=O, and O–H, which remained on GO after catalyst preparation [35]. As the temperature increased to 600°C, more than 70% of the mass was lost due to the decomposition of the remaining stable oxygen functionalities and the carbon component [36]. These results indicated the presence of oxygen functional groups on the Pd/GO after the catalyst preparation. Beyond 650°C, all catalysts remained at a ~5% weight, which was assigned to the wt% of Pd loading on the carbonaceous supports. The FT-IR spectra were also collected to identify the major oxygen functional groups present on the prepared Pd-based catalysts. As shown in Figure 3 (Right panel), the peak assigned to the O–H bond stretching at 3429 cm^{-1} was present in all samples. Peaks corresponding to the C=C bond stretching of the graphite structure at 1620 cm^{-1} were detected in the Pd/AC and Pd/CNT catalysts, whereas a peak at 1556 cm^{-1} in the Pd/GO catalyst spectrum was attributed to the skeletal vibrations of the graphene sheets [37]. Furthermore, the FT-IR spectrum of the Pd/GO catalyst showed additional bands at 1054 cm^{-1}, 1224 cm^{-1}, and 1697 cm^{-1}, which were attributed to carboxylate C–O, epoxide C–O–C, and carboxyl C=O stretching vibrations, respectively. It is worth noting that the absorption bands of the Pd/GO catalyst were more intense than the bands collected from the other samples due to the large number of oxygen functional groups present on the GO after the catalyst preparation steps. The FT-IR spectra indicated that the Pd/GO catalyst contained a larger variety of oxygen functional groups compared to the other samples, consistent with the TGA data.

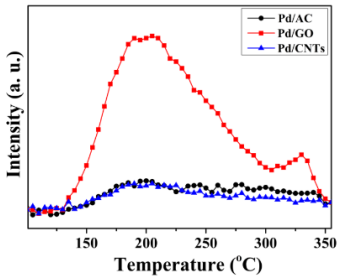

Figure 4. NH_3-TPD analysis of the prepared Pd-based catalysts: (black) Pd/AC, (red) Pd/GO, and (blue) Pd/CNTs.

The oxygen functional groups observed in the TGA and FT-IR analyses were further characterized using the temperature-programmed desorption of ammonia (TPD–NH_3) technique to measure the quantity as well as strength of the acidic sites present on the synthesized Pd-based catalysts. The kinetic diameter of an NH_3 molecule is sufficiently small (0.26 nm) to diffuse through narrow pores, adsorb onto the surfaces of the catalysts, and react with Brønsted and Lewis acid sites. Although the data obtained from TPD–NH_3 analysis could not distinguish between the Brønsted and Lewis acid groups [38], it provided comparative information about the surface acidity of each catalyst. Conventionally, acidic sites are classified based on the desorption temperature range, where weak sites desorb at 120°C–250°C, medium sites desorb at 250°C–400°C, and strong sites at >400°C [39].

In the present work, the TPD–NH_3 studies were conducted only up to 350°C due to the instability of the carbonaceous materials at higher temperatures, as indicated by the TGA data. Figure 4 shows that the Pd/GO catalyst exhibited an intensely broad desorption signal ranging from 120°C to 300°C and a narrower but tailing signal in the range 300°C–350°C. These signals were attributed to desorption from weak and medium acidic sites, respectively. Moreover, the TPD–NH_3 profiles revealed that both the weak and medium acidic sites on the Pd/GO catalyst were present in significant excess of those present on the Pd/AC and Pd/CNTs catalysts. The total concentration of acidic sites

present on the Pd/GO catalyst was calculated to be 134.76 μmolg^{-1}, 6.5 times the concentration of acidic sites present on the Pd/AC catalyst and 7.3 times that present on the Pd/CNTs catalyst. The acidic sites on the Pd/GO catalyst originated from the oxygen functional groups that remained after the catalyst preparation steps, further confirm the previous data.

3.2. Asymmetric hydrogenation reaction of PCA

Metal surfaces in asymmetric heterogeneous hydrogenation systems act as the active sites for reactions, whereas chiral modifiers generate chiral sites *via* adsorption onto the metal surface [40]. After protonation, the modifier CD molecule adsorbs onto the Pd surface in a suitable mode to provide a chiral environment and subsequently interacts with the substrate *via* hydrogen bonds to form intermolecular complexes that finally produces products with enantiodifferentiation [41,42]. The pretreatment procedure is performed to remove oxygen and impurities from the Pd surface, which enhances enantioenrichment by increasing the number of adsorbed CD molecules and also favoring the adsorption of CD on the Pd surface in the suitable mode [31].

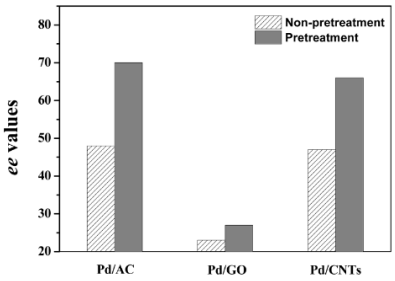

Figure 5. *ee* values obtained from the prepared Pd-based catalysts: Pd/AC, Pd/GO and Pd/CNTs.

As shown in Figure 5, the *ee* values obtained from the Pd/AC and Pd/CNTs catalysts were modest, 48%, in the non-pretreatment case. The pretreatment procedure significantly enhanced the enantioselectivity to values of 70% and 66%, respectively. The *ee* values attained from the Pd/AC and Pd/CNTs catalysts suggested that the structural morphologies of the supports only trivially influenced the enantioselective performance. On the other hand, the prepared Pd/GO catalyst displayed an *ee* of only 23% in the non-pretreatment case, which was very poor compared with the values obtained from the other catalysts. Moreover, the pretreatment procedure only enhanced the *ee* up to 27%. The similar drop of *ee* values obtained from the Pd/GO catalyst submitted to both procedures suggested that the purified Pd nanoparticle surface after the pretreatment procedure was essentially impervious to improving the *ee*. Instead, the quantity of CD molecules adsorbed onto the Pd surface and their adsorption mode were decisive in determining the *ee*. In other words, CD molecules did not favorably adsorb onto the Pd surface, regardless of the removal of contaminants on the surface. Under conditions that did favor adsorption onto the Pd surface, the CD molecules did not adsorb in the suitable mode to induce enantioselectivity.

The support polarity has been shown to affect the catalytic performance in a variety of reactions [43–45]. These effects have been ascribed to variations in the adsorbed reactant quantities due to the presence of oxygen functional groups on the support surface, which promote or reduce the desired products. Protonated amine groups adsorbed onto the GO support appear to incorporate themselves between the negatively charged carboxylate functional groups remaining on the reduced graphene surface after chemical reduction and the positively protonated amine groups *via* attractive electrostatic interactions. This binding mode has been supported by both theoretical calculations [46] and experimental data [47].

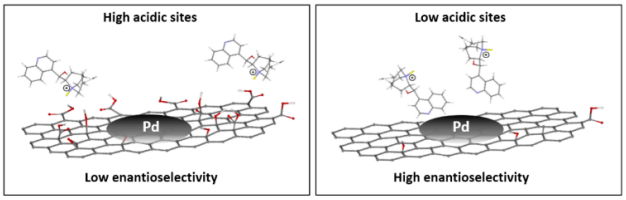

Scheme 1. Schematic diagram showing the influence of oxygen functional groups on the enantioselective hydrogenation of PCA.

The effects of the support polarity and the abundance of acidic sites present on the Pd/GO catalyst suggest that the low *ee* values measured from the Pd/GO catalyst were associated with oxygen-containing groups present on the catalyst surface. In other words, the negatively charged oxygen functional groups present on the GO surface of the prepared Pd/GO catalyst might attract or even interact with the positively protonated quinuclidine nitrogen moiety in the CD molecule *via* electrostatic forces (Scheme 1). These effects could alter the adsorption mode of CD on the Pd surface in the former case, or favor the preferential adsorption of CD on the GO surface in the latter case. This, in turn, decreased the quantity of modifier–substrate intermediate complexes that could produce enantioselectivity, leading to an inevitable drop in the *ee* values.

4. CONCLUSION

We investigated the influence of the catalyst support on the enantioselectivity of the asymmetric heterogeneous hydrogenation of PCA in a comparative study of Pd-based catalysts supported on carbonaceous materials (AC, GO, or CNTs). The Pd-based catalysts were prepared by the deposition method and were characterized using a variety of methods. The results suggested that the morphologies of the catalyst supports did not significantly affect the *ee* value. The Pd/GO catalyst, which contained an abundance of acidic sites relative to the other catalysts due to the presence of oxygen functional groups after the catalyst preparation, induced very low *ee* values in the hydrogenation of PCA. The results suggest that the support acidity reduced the *ee* value by favoring the preferential adsorption mode of CD molecules on the GO surface *via* electrostatic interactions.

REFERENCES

[1] A. Villa, M. Schiavoni, L. Prati, *Catal. Sci. Tech.* **2012**, *2*, 673.
[2] G. Agostini, C. Lamberti, R. Pellegrini, G. Leofanti, F. Giannici, A. Longo, E. Groppo, *ACS Catal.* **2014**, *4*, 187.
[3] F. Cárdenas-Lizana, Y. Hao, M. Crespo-Quesada, I. Yuranov, X. Wang, M. A. Keane, L. Kiwi-Minsker, *ACS Catal.* **2013**, *3*, 1386.
[4] F. Rodríguez-reinoso, *Carbon* **1998**, *36*, 159.
[5] X. Peng, J. Chen, J. A. Misewich, S. S. Wong, *Chem. Soc. Rev.* **2009**, *38*, 1076.
[6] C. N. R. Rao, A. K. Sood, K. S. Subrahmanyam, A. Govindaraj, *Angew. Chem. Int. Ed.* **2009**, *48*, 7752.
[7] B. Wu, Y. Kuang, X. Zhang, J. Chen, *Nano Today* **2011**, *6*, 75.
[8] B. Luo, S. Liu, L. Zhi, *Small* **2012**, *8*, 630.
[9] H. F. Stoeckli, *Carbon* **1990**, *28*, 1.
[10] I. A. A. C. Esteves, F. J. A. L. Cruz, E. A. Müller, S. Agnihotri, J. P. B. Mota, *Carbon* **2009**, *47*, 948.
[11] D. R. Dreyer, S. Park, C. W. Bielawski, R. S. Ruoff, *Chem. Soc. Rev.* **2010**, *39*, 228.
[12] K. Borszeky, T. Mallat, A. Baiker, *Tetrahedron: Asymmetry* **1997**, *8*, 3745.
[13] G. Szöllősi, K. Balázsik, M. Bartók, *Appl. Catal. A* **2007**, *319*, 193.
[14] G. Szöllősi, E. Szabó, M. Bartók, *Adv. Synth. Catal.* **2007**, *349*, 405.
[15] Y. Nitta, Y. Ueda, T. Imanaka, *Chem. Lett.* **1994**, *23*, 1095.
[16] Y. Nitta, K. Kobiro, *Chem. Lett.* **1995**, *24*, 165.
[17] G. Szőllősi, B. Hermán, K. Felföldi, F. Fülöp, M. Bartók, *J. Mol. Catal. A: Chem.* **2008**, *290*, 54.
[18] T. Sugimura, T. Uchida, J. Watanabe, T. Kubota, Y. Okamoto, T. Misaki, T. Okuyama, *J. Catal.* **2009**, *262*, 57.
[19] Y. Nitta, T. Kubota, Y. Okamoto, *J. Mol. Catal. A: Chem.* **2004**, *212*, 155.
[20] T. Y. Kim, T. Sugimura, *J. Mol. Catal. A: Chem.***2010**, *327*, 58. [21] T. Kubota, H. Ogawa, Y. Okamoto, T. Misaki, T. Sugimura, *Appl. Catal. A* **2012**, *437–438*, 18.
[22] T. Sugimura, J. Watanabe, T. Okuyama, Y. Nitta, *Tetrahedron: Asymmetry* **2005**, *16*, 1573.
[23] T. Sugimura, J. Watanabe, T. Uchida, Y. Nitta, T. Okuyama, *Catal. Lett.* **2006**, *112*, 27.
[24] T. Y. Kim, M. Yokota, T.; Uchida, T. Sugimura, *Catal. Lett.* **2009**, *131*, 279.
[25] T. Sugimura, H. Ogawa, *Chem. Lett.* **2010**, *39*, 232.
[26] K. Szőri, R. Puskás, G. Szőllősi, I. Bertóti, J. Szépvölgyi, M. Bartók, M. *Catal. Lett.* **2013**, *143*, 539.
[27] Z. Guan, S. Lu, C. Li, *J. Catal.* **2014**, *311*, 1.
[28] V. C. Tung, M. J. Allen, Y. Yang, R. B. Kaner, *Nat. Nanotechnol.* **2009**, *4*, 25.
[29] M. L. Toebes, J. A. van Dillen, K. P. de Jong, *J. Mol. Catal. A: Chem.* **2001**, *173*, 75.
[30] S. Louis, H. J. Merritt (1958). *"Method of preparing hydrogenation catalysts"* U.S. Patent 2,857,337 A, Oct 21, 1958.
[31] Y. Nitta, J. Watanabe, T. Okuyama, T. Sugimura, *J. Catal.* **2005**, *236*, 164.
[32] S. Yang, C. Shen, Y. Tian, X. Zhang, H. J. Gao, *Nanoscale* **2014**, *6*, 13154.
[33] B. Fultz, J. Howe (2013) *Transmission Electron Microscopy and Diffractometry of Materials*; Springer Berlin Heidelberg, 2013; p 1.
[34] G. J. Thomas, R. W. Siegel, J. A. Eastman, *Mat. Res. Soc. Symp. Proc.* **1989**, *153*, 13.
[35] S. Stankovich, D. A. Dikin, R. D. Piner, K. A. Kohlhaas, A. Kleinhammes, Y. Jia, Y. Wu, S. T. Nguyen, R. S. Ruoff, *Carbon* **2007**, *45*, 1558.
[36] T. Zhou, F. Chen, K. Liu, H. Deng, Q. Zhang, J. Feng, Q. Fu, *Nanotechnol.* **2011**, *22*, 045704.
[37] S. Park, J. An, I. Jung, R. D. Piner, S. J. An, X. Li, A. Velamakanni, R. S. Ruoff, *Nano Lett.* **2009**, *9*, 1593.
[38] M. Niwa, N. Katada, *Chem. Record* **2013**, *13*, 432.
[39] A. Boréave, A. Auroux, C. Guimon, *Microporous Mater.* **1997**, *11*, 275.
[40] T. Mallat, E. Orglmeister, A. Baiker, *Chem. Rev.* **2007**, *107*, 4863.
[41] Y. Nitta, A. Shibata, *Chem. Lett.* **1998**, *27*, 161.
[42] G. Kyriakou, G.; S. K. Beaumont, R. M. Lambert, *Langmuir* **2011**, *27*, 9687.
[43] X. Wang, N. Li, J. A. Webb, L. D. Pfefferle, G. L. Haller, *Appl. Catal. B* **2010**, *101*, 21.
[44] M. L. Toebes, Y. Zhang, J. Hájek, T. Alexander Nijhuis, J. H. Bitter, A. Jos van Dillen, D. Y. Murzin, D. C. Koningsberger, K. P. de Jong, *J. Catal.* **2004**, *226*, 215.
[45] R. W. Gosselink, W. Xia, M. Muhler, K. P. de Jong, J. H. Bitter, *ACS Catal.* **2013**, *3*, 2397.
[46] D. Stauffer, N. Dragneva, W. B. Floriano, R. C. Mawhinney, G. Fanchini, S. French, O. Rubel, *J. Chem. Phys.* **2014**, *141*, 044705.
[47] E. Y. Choi, T. H. Han, J. H. Hong, J. E. Kim, S. H. Lee, H. W. Kim, S. O. Kim, *J. Mater. Chem.* **2010**, *20*, 1907.